ATIC AEROACOUSTIC MODEL ROTOR TEST AT DNW

Atsushi Murashige , Noboru Kobiki , Akihiko Tsuchihashi ,
Hideaki Nakamura , Kenjiro Inagaki , Eiichi Yamakawa

ATIC (Advanced Technology Institute of Commuter-Helicopter, Ltd.)
2 Kawasaki-cho, Kakamigahara City, Gifu Pref., 504-0971 Japan

Abstract

This paper presents the major topics evaluated by ATIC model rotor test performed at DNW from Jan.23rd to Mar.6th, 1998. In this test, the performance and the aeroacoustic data were obtained for 3 types of blades (baseline blade and 2 advanced blades) under the level flight conditions (μ =0~0.34) and the descent flight conditions (μ =0.12~0.2). The parametric study of HHC (Higher Harmonic Control) effect on the BVI (Blade Vortex Interaction) noise was also investigated. On the BVI condition at μ =0.16, the flow visualization of the tip vortex was performed using LLS (Laser Light Sheet) and PIV (Particle Image Velocimetry) techniques. The blade deformation data was also measured by PGM (Projected Grid Method) with HHC-on/off cases. Based on the obtained results in this model rotor test, the effects of variable rotor rpm, number of blades, blade geometry and HHC on the rotor performance and noise are discussed in this paper.

Notation

Symbols

c	Blade chord length=110.7mm
r	Blade local spanwise station(m)
R	Rotor radius =2m

Coordinate system centered at rotor center

x	positive in downstream direction
y	positive in starboard direction
z	positive in upward direction
C_p	Pressure coefficient defined as ; $C_p = \frac{p_{total} - p_{static}}{\frac{1}{2}\rho(\Omega r)^2}$
C_T	Thrust coefficient
C_Q	Torque coefficient
V	Wind tunnel speed (m/sec)
α	Rotor angle of attack(positive in nose up direction)
μ	Advance ratio
ϕ	Rotor azimuth angle (deg.)
ϕ_{HHC}	HHC phase angle (deg.) which is defined as the rotor azimuth angle where the blade pitch angle becomes its minimum as below.
Ω	Rotor rotational speed(rad/sec)
ρ	air density

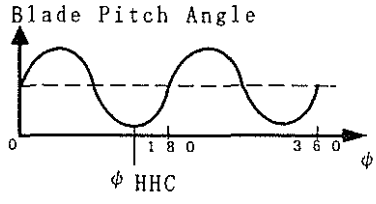

Abbreviations/Subscripts

BVI	Blade Vortex Interaction
HHC	Higher Harmonic Control
LLS	Laser Light Sheet
PGM	Projected Grid Method
PIV	Particle Image Velocimetry
OSPL	Over all Sound Pressure Level(dB)
SPL	Sound Pressure Level(dB)

Introduction

Although civil helicopter has been strongly expected to play a very significant role in Japan where the terrain is mountainous and the plain is highly populated, the noise problem especially around the residential area and the concern for operational safety prevented helicopters from being prevalent in Japan.

ATIC was established in 1994 to research and develop the technologies in aeroacoustic area to reduce helicopter external noise and in flight safety area.
The major aeroacoustic research items which ATIC has been conducting are as follows;

a)prediction technique of rotor noise and performance (Refs.1,2)
b)airfoil and tip planform (Refs.3,4)
c)design trade-study for optimization between noise and performance
d)HHC and active flap for noise and vibration reduction (Refs.5,6,7)
e)variable rotor rpm system
f)BVI noise analysis (Refs.8,9)
g)flow visualization techniques (LDV and PIV) (Refs.10,11)

To evaluate these research items comprehensively and to construct a data base for analytical code validation, ATIC conducted the wind tunnel testing at DNW in the beginning of 1998.

This paper presents the major results of this DNW testing as the first report.

Objectives

The main objectives of the ATIC model rotor test at DNW are as follows.

(1)Evaluate the effect of the following items on rotor performance, acoustic noise and vibration in the wind tunnel testing.

- Blade Geometry : Airfoil and Tip Shape
- Number of Blades
- Variable Rotor Rpm
- HHC

(2)Data collection for aeroacoustic and aeroelastic codes validation by the wind tunnel testing

Test Description at DNW

(1)ATIC Model Rotor System

The general specification of ATIC model rotor system is shown in Table 1. See Ref.12 for more details .

The rotor system was set in the open jet configuration as shown in Fig.1.

Table1 Primary Feature of ATIC Model Rotor System

Rotor	blade	dynamically scaled 2m radius,110.7mm chord tip:baseline, type-1 and type-2 linear twist of -8 deg
	hub	fully articulated 4 bladed and 5 bladed
Rotor drive system		hydraulic 200HP output
Primary blade pitch control		collective:-6 to +18deg. @75%r/R cyclic:-15 to +15deg.
HHC		amplitude:0.8deg. @105Hz frequency:up to 105Hz phase shift:variable
Signal conditioning		256ch pre-amp. on the rotating frame
Data acquisition system		256ch simultaneous measuring and on-line data processing capability data band width up to 20kHz
Operating condition		rotor rpm:840 to 1050rpm max. thrust:800kgf max. rotor shaft torque: 140kgfm

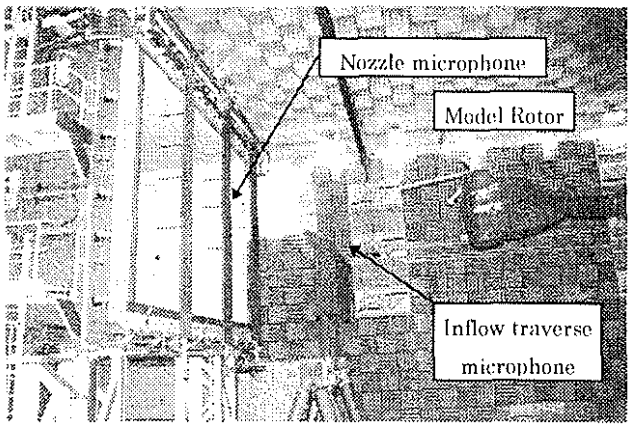

Fig.1 Model rotor setup in DNW

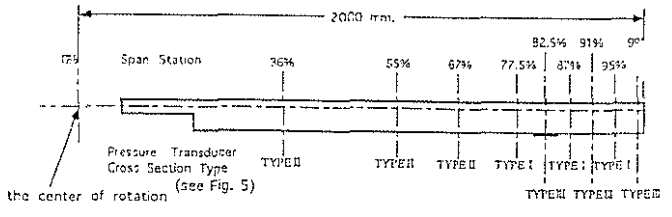

Baseline blade

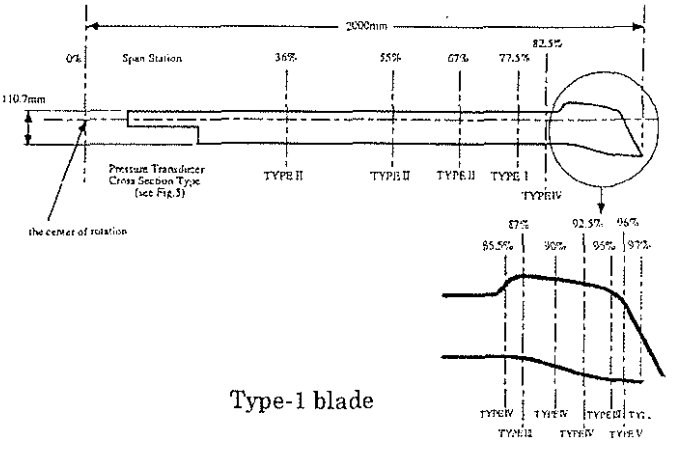

Type-1 blade

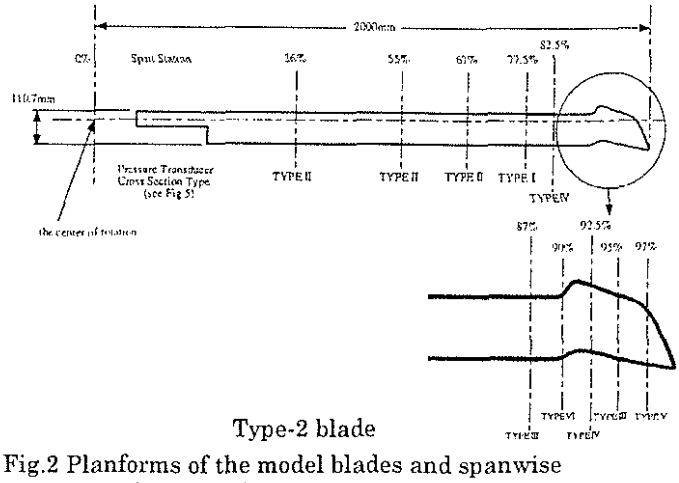

Type-2 blade

Fig.2 Planforms of the model blades and spanwise distributions of pressure transducers

(2)Model Blades

Three types of rotor blades were evaluated; baseline(rectangular), type-1 (BERP like) and type-2(AT1). Each of them has a 4 meter diameter with a nominal blade chord of 110.7mm and a linear twist of -8deg.

The airfoil section of the baseline blades is NACA23012mod. Both of type-1and-2 blades have the same airfoil section; an AK100D tapering to an AK080A at the tip section outboard of r=1600(mm).

Each of the three types contains one pressure instrumented blade with approximately 100 pressure transducers and two heavily strain gage instrumented blades with about 20 strain gages to measure the blade load/deformations. The planform of each blade and the location of sensors are shown in Fig.2 to Fig.4.

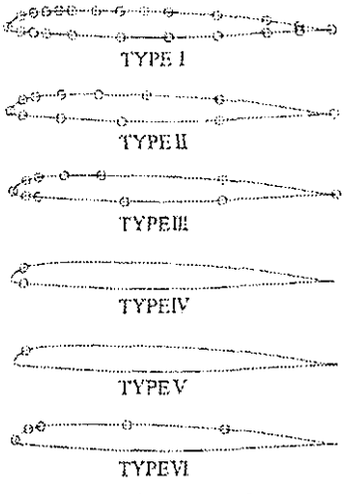

Fig.3 Chordwise distributions of pressure traducers at spanwise locations (common to 3 types of blades)

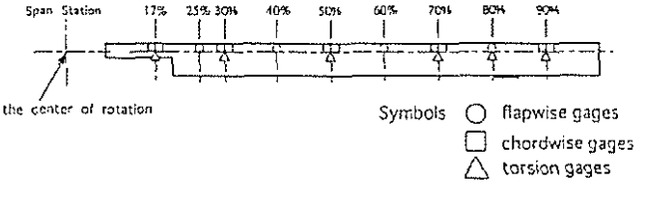

Fig.4 Spanwise distributions of strain gages (common to 3 types of blades)

(3)Test Case

A lot of test cases were carried out to evaluate the effects of the variable rotor rpm, the number of blades, the blade tip shapes and HHC. The test conditions at each test case are shown in Fig.5(a),(b) . The contents of each test are as follows;

(a)Acoustic and Performance

The acoustic and the performance data were measured under the various flight conditions including hover,1G level flight, and α sweep in the middle flight speed range.

For the rotor noise measurement, 27 microphones in total were used. The 12 microphones were set at the wind tunnel nozzle to measure the noise propagation in forward direction. The other 13 microphones were installed on the inflow microphone traverse system (maximum traverse range was x=±4m) to get the carpet plot 2.3m below the rotor. The other 2 microphones were installed on both sides of the rotor test rig.

For studying the effect of number of the blades, only the baseline blade was used.

All the three types of the blades were used for the study of the variable rotor rpm effect, the thrust effect and the blade geometry effect,.

During this test period, the blade surface pressure data was also measured, which was required for the validation of the CFD software developed by ATIC.

(b)HHC

For the basic understanding of the HHC effects on the rotor noise and the vibration, the parametric study of the HHC input parameters was performed using the baseline blade in 5-bladed configuration. In this test, the performance data, the acoustic data and the vibration data were measured under the BVI condition of the descent flight. (V=33.4m/s, α =4.72 ° , CT=0.0064, Rotor RPM=1003rpm)

(c)Tip Vortex Flow Visualization

The tip vortex trajectories of baseline blade and type-2 blade were measured by LLS. The flow velocity fields around the tip vortex was also measured by PIV.

This test was conducted on the BVI condition of the descent flight. (V=33.4m/s, α=4.72° , CT=0.0064, Rotor RPM=1003rpm)

In the baseline blade case, the HHC effects on the tip vortex trajectories and the tip vortex velocity fields were also studied by use of LLS and PIV, respectively.

(d)Blade Deformation

The deformation data of the baseline blade in HHC on/off cases were obtained by the PGM method. The test condition was the same as above mentioned two tests.((b) and (c))

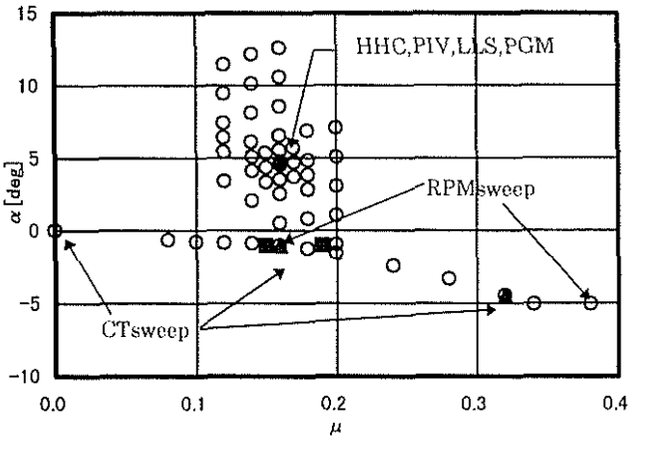

Fig.5(a) Test cases (μ - α plot)

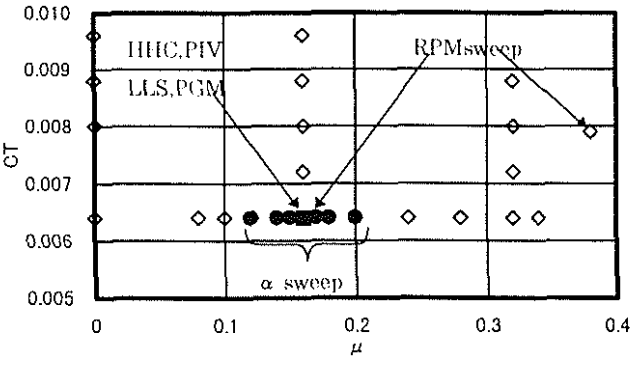

Fig.5(b) Test cases (μ -CT plot)

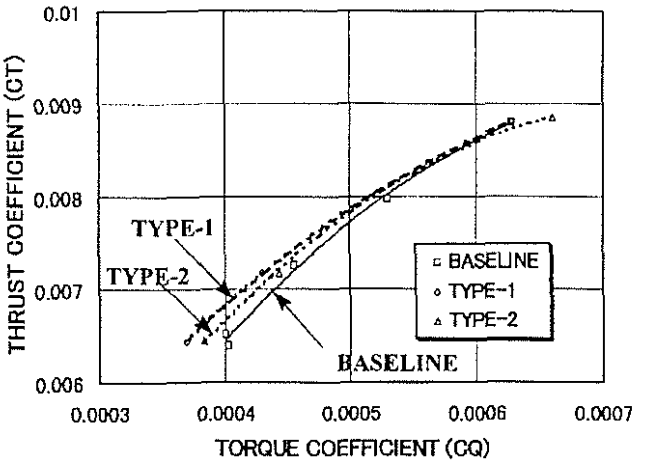

Fig.7 Rotor performance of 3 types of blades on the high speed condition
test condition: μ =0.32, α =-4.45° ,
R Ω=210m/s,CT=0.0064～0.0088

Test Results

(1)Rotor Performance

Fig.6 shows the level flight performance of three types of blades at the nominal thrust level (CT=0.0064).

As seen from this figure, while the baseline blade is the best in performance on the low wind speed condition, the type-1 blade is the best on the high wind speed condition.

The type-2 blade shows the good performance all over the speed range, having both benefits of the baseline blade in the low speed region and the type-1 blade in the high speed region.

Fig.7 is the CT-CQ curve of each blade on the high wind speed condition (μ =0.32). From this figure, it can be seen that the performance of the type-1 and the type-2 blade is better than that of the baseline blade in this order at the lower thrust level. However, as the rotor thrust level increases, the difference of the performance among these three blades decreases.

The reason of this tendency is not certain at present. But, further investigation will be requested based on the blade surface pressure information for the understanding of this phenomenon.

(2)Variable Rotor Rpm Effect on Rotor Noise

Fig.8 shows the spectra of the out-of-plane rotor noise at 3 rotor rotational speeds (859rpm, 1003rpm, 1050rpm) on the middle speed level flight condition (μ =0.16, α =-1.01). The rotor thrust level is maintained to 444 kgf in all rotor rpm cases. The microphone position is just below the advancing side of the rotor (x/R=0, y/R=0.9, z/R=-1.15). As shown in this figure, the rotor rotational speed has very little effect on the out-of-plane rotor noise, especially in the frequency

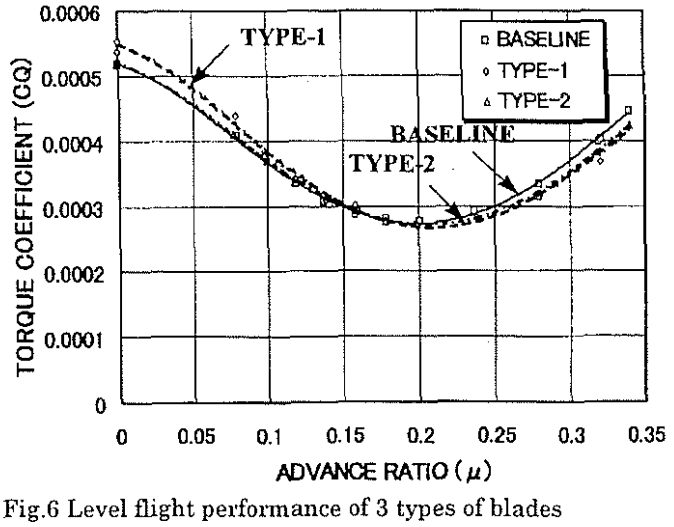

Fig.6 Level flight performance of 3 types of blades
test condition: μ =0～0.34, α is set to calculated trim,
R Ω=210m/s, CT=0.0064

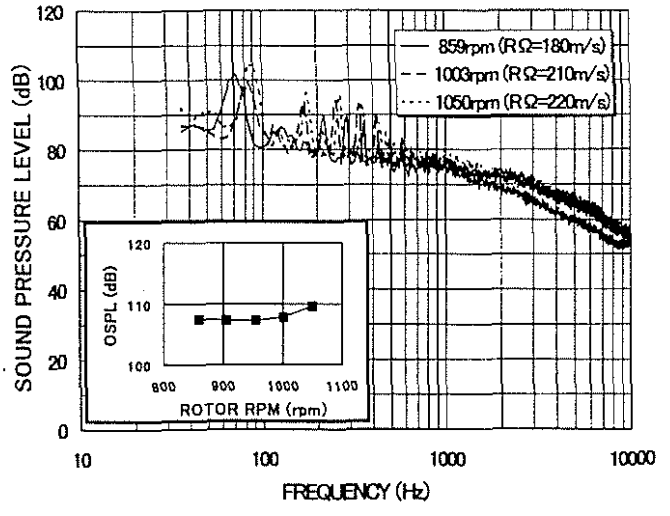

Fig.8 Effect of rotor rotational speed on the out-of-plane rotor noise
test condition: μ =0.16, α =-1.01° , CT=0.0064
R Ω=180～220m/s (859～1050rpm)
microphone : x/R=0, y/R=0.9, z/R=-1.15

range under 1000 Hz.

As for the broadband noise in the frequency range over 1000 Hz, the strong dependency on the rotor rpm can be recognized.

Fig.9 shows the variable rotor rpm effect on the spectra of the in-plane rotor noise. The test condition is the same as in Fig.8. The microphone position is the right-front of the rotor (x/R=-3.57, y/R=1.28, z/R=0).

As shown in this figure, the strong dependency of the in-plane noise on the rotor rotational speed can be seen all over the noise frequency range.

From these results about the out-of-plane and the in-plane noise, the noise reduction by the variable rpm can be expected only for the in-plane rotor noise.

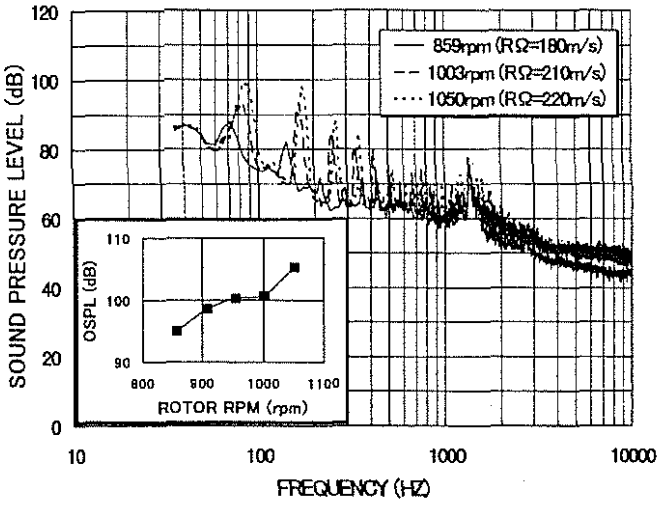

Fig.9 Effect of rotor rotational speed on the in-plane rotor noise
test condition: μ =0.16, α =-1.01° ,CT=0.0064
R Ω=180～220m/s (N=859～1050rpm)
microphone :x/R=-3.57, y/R=1.28, z/R=0

(3)Number of Blades Effect on Rotor Noise

Fig.10 shows one example of the effect of number of blades on the rotor noise under the constant thrust conditions.

The OSPL of the out-of-plane rotor noise is presented for the 4-bladed and the 5-bladed rotor as the function of the rotor angle of attack. The microphone position is just below the advancing side of the rotor (x/R=0, y/R=0.9, z/R=-1.15).

From this figure, we can see that the OSPL of the 4-bladed rotor is 2 to 3 dB higher than that of the 5-bladed rotor at the wide range of angle of attack. At higher angle of attack than 6 deg., however, no difference can be observed between the 4-bladed and the 5-bladed rotor.

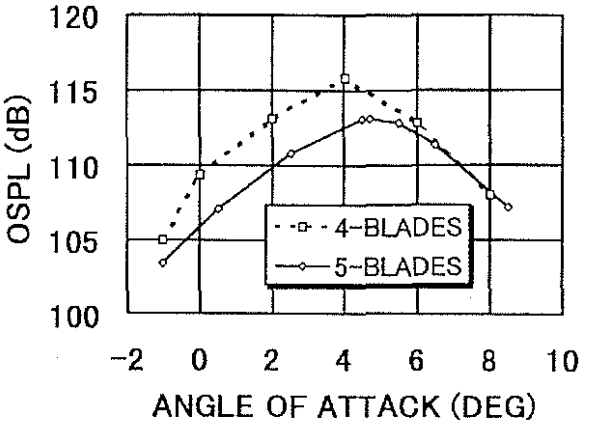

Fig.10 Effect of number of blades on the out-of-plane rotor noise
test condition: μ =0.16, α =-1～8° ,CT=0.0064
R Ω=210m/s
microphone : x/R=0, y/R=0.9, z/R=-1.15

Fig.11 shows the carpet plots of mid-frequency band noise of 355Hz to 5.6kHz range for the 4-bladed and the 5-bladed rotor. These data are obtained by the inflow traverse microphone on the maximum BVI condition (μ =0.16, α =4° , CT=0.0064).

From this figure, the peak noise level and the size of the strong noise region are affected by the number of blades. The peak SPL of the 5-bladed rotor is about 2dB lower than that of the 4-bladed rotor in both BVI regions of advancing and retreating sides.

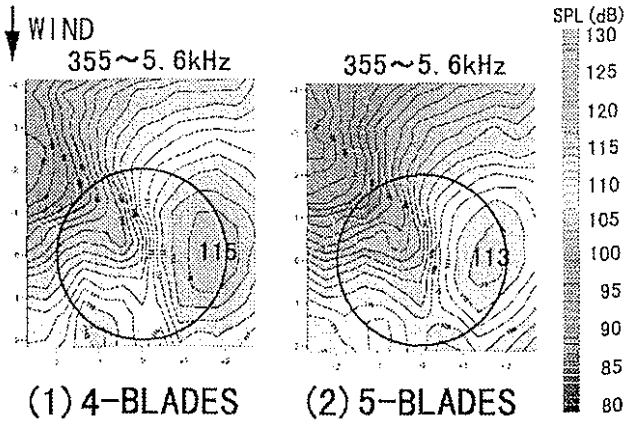

Fig.11 Effect of number of blades on the BVI noise
test condition: μ =0.16, α =-1～8° ,CT=0.0064
R Ω=210m/s
microphone : inflow traverse microphone (z/R=-1.15)

From these results, it is inferred that the improvement of the out-of plane rotor noise level by 5-bladed rotor comes from the lower blade aerodynamic load caused by the lower blade loading. Because the lower blade load has the possibility to reduce BVI noise by relieving the degree of pressure fluctuation on the blade during BVI. Further data evaluation is required to understand the disappearance of this effect more than α=6deg..

(4)Blade Geometry Effect on Rotor Noise

Fig.12 shows the in-plane rotor noise spectra of 3 types of blades measured by the nozzle microphone (x/R=-3.57, y/R=1.28, z/R=-0.38) on the low speed level flight condition (μ=0.08, α=-0.66° , CT=0.0064).

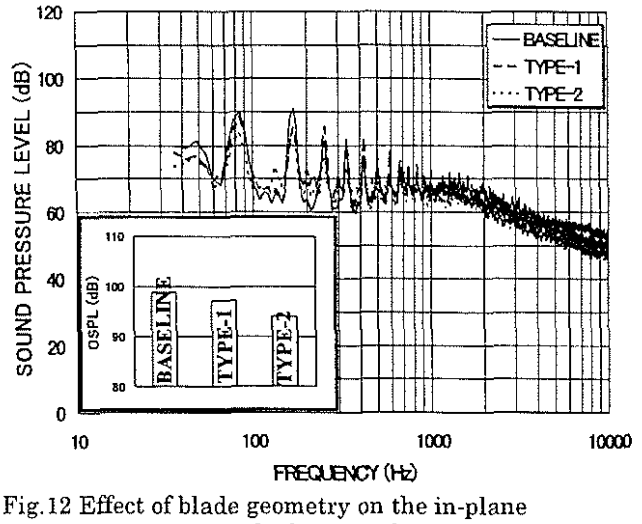

Fig.12 Effect of blade geometry on the in-plane rotor noise on the low speed condition
test condition: μ=0.08, α=-0.66° ,CT=0.0064, R Ω=210m/s
microphone : x/R=-3.57, y/R=1.28, z/R=0.38

As seen from Fig.12, the noise level of the type-2 blade is the lowest all over the frequency range. The worst is the baseline blade and the type-1 blade is in between.

Fig.13 shows the rotor in-plane noise spectra of three types of blades measured by the nozzle microphone (x/R=-3.57, y/R=1.28, z/R=-0.38) on the high speed level flight condition (μ=0.34, α=-5.05° , CT=0.0064).

As shown in this figure, the difference among each blade is very small. Because we expected the lower noise level would be observed in the type-1 and the type-2 blade case than in the baseline blade, this result is contrary to our expectation.

To understand the reason of this result, further investigation will be continued.

Fig.14 shows the carpet plots of the mid frequency band noise of three types of blades, which is obtained by the inflow traverse microphones on the descent flight

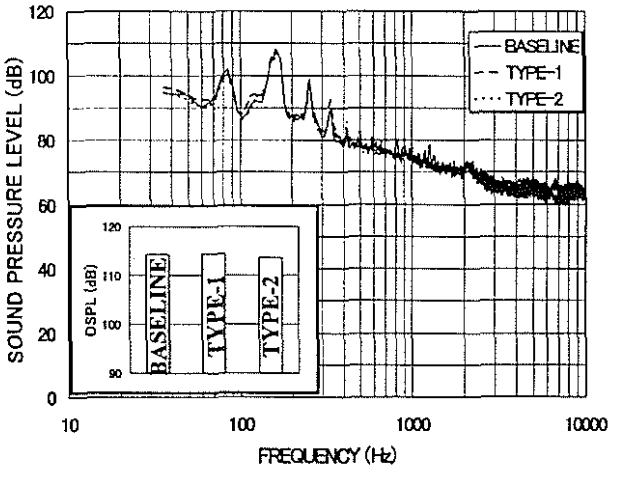

Fig.13 Effect of blade geometry on the in-plane rotor noise on the high speed condition
test condition: μ=0.34, α=-5.05° ,CT=0.0064, R Ω=210m/s
microphone : x/R=-3.57, y/R=1.28, z/R=-0.38

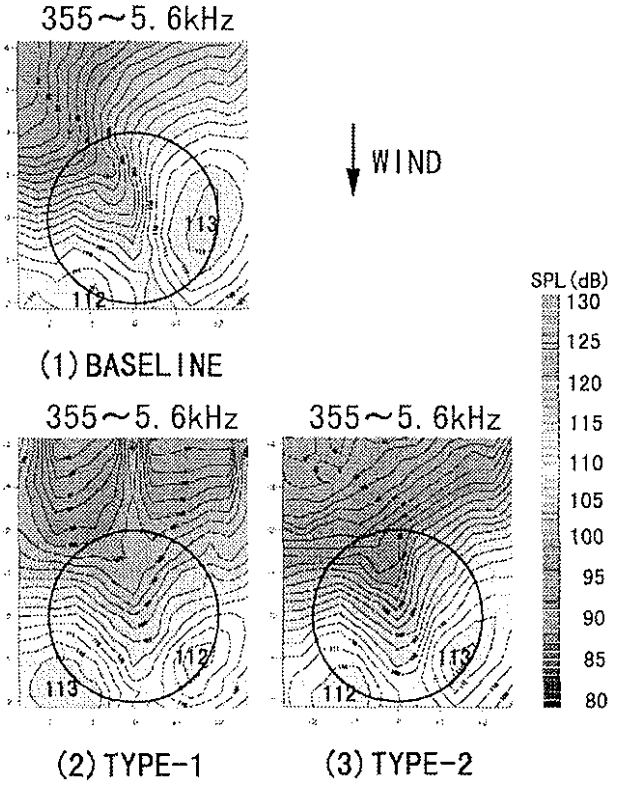

Fig.14 Effect of blade geometry on the BVI noise
test condition: μ=0.16, α=4.72° ,CT=0.0064 R Ω=210m/s
microphone : inflow traverse microphone (z/R=-1.15)

condition (μ =0.16, α =4.72° ,CT=0.0064).

The upper plot is the carpet plot of the baseline blade, the lower left one is that of the type-1 blade and the lower right one is that of the type-2 blade. As seen from this figure, the position and the size of the high SPL region is influenced by the blade geometry.

In the type-1 and the type-2 blade case, the advancing side high SPL region is observed at the smaller azimuth position than in the baseline blade case.

And the size of this high SPL region is decreased on both blade cases compared to the baseline blade case. To understand the reason why the blade geometry affects the BVI noise, we try the PIV and the LLS to the baseline and the type-2 blade.

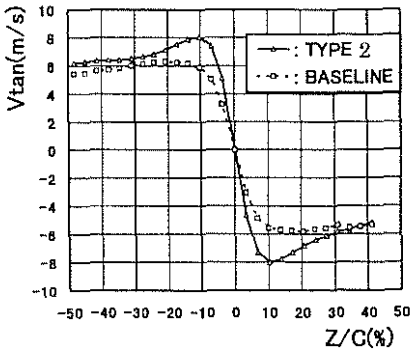

Fig.-15 Tangential velocity distribution in the tip vortex of 2 types of blades
test condition: μ =0.16, α =4.72° ,CT=0.0064
R Ω =210m/s

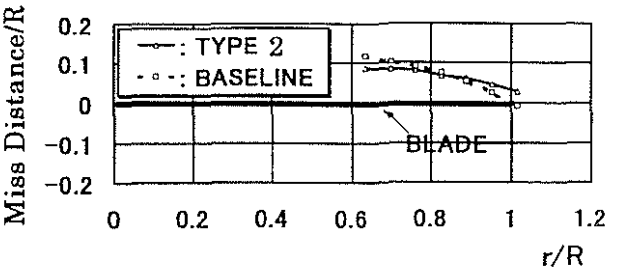

Fig.16 Blade/vortex miss distance of 2 types of blades
test condition: μ =0.16, α =4.72° ,CT=0.0064
R Ω =210m/s

Fig.15 shows the velocity distribution of the tip vortex measured by PIV and Fig.16 shows the blade/vortex miss distance measured by LLS.

From Fig.15, we can see the tip vortex strength of the type-2 blade is stronger than that of the baseline blade contrary to our expectation.

From Fig.16, the miss distance of type-2 blade in the blade tip region, where the large BVI noise is generated, is lager than that of the baseline blade.

The type-2 blade has the lower noise in spite of higher vortex strength than the baseline blade. This can be explained that the type-2 blade has a larger miss distance at the blade tip region than the baseline blade has. We think the future work for evaluating the test data with various test condition will give us the sufficient insight for quantifying the effect of blade geometry on the rotor noise.

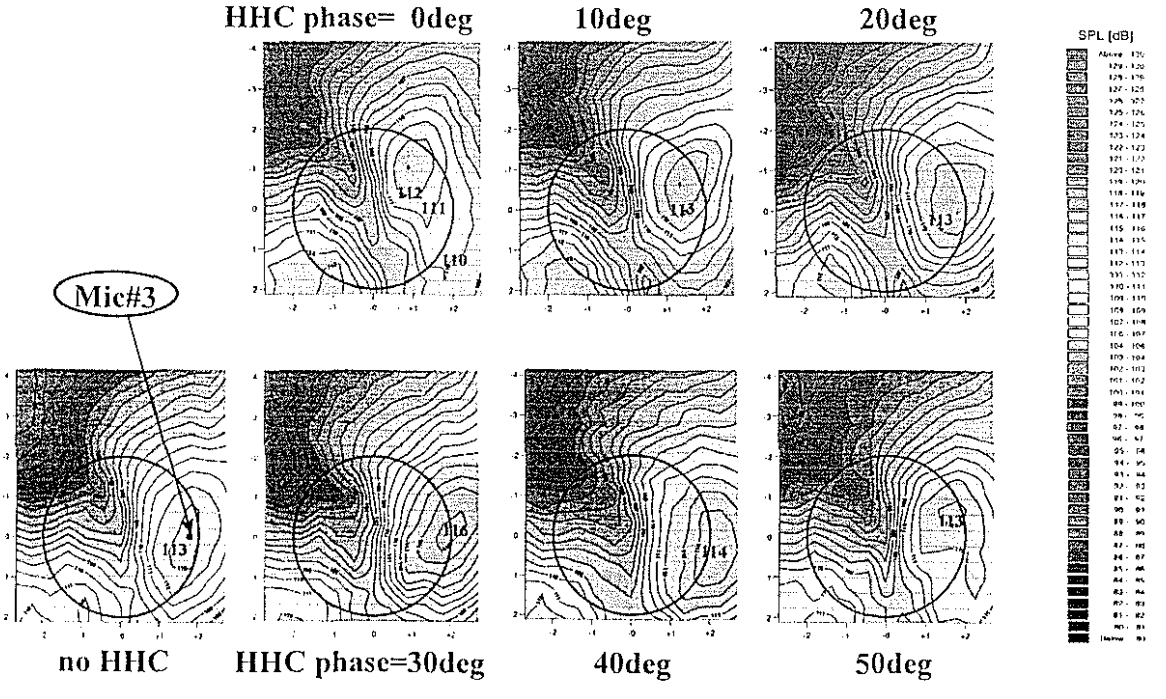

Frequency band : Mid freq=355 to 5,600Hz

Fig.17 HHC effect on BVI noise in the flow traverse microphone SPL carpet plot
6/rev HHC, amp.=0.4deg

(5) HHC

The effect of HHC on BVI noise reduction is evaluated applying 6/rev HHC to the 5 bladed rotor.

The carpet plot of the mid frequency band (355 to 5600Hz) containing BVI noise obtained by the inflow traverse microphone is shown in Fig.17.

The high SPL regions caused by BVI noise propagation can be observed on both advancing and retreating sides in each ϕ_{HHC} case as well as no HHC case. But the BVI noise is reduced by HHC with ϕ_{HHC}= around 0deg.

In order to evaluate HHC effect in more detail by the sound pressure spectrum, Mic#3 at the position illustrated in Fig.17 is selected as reference.

Fig.18 shows HHC influence on mid frequency SPL represented by over all value of Mic#3. There can be seen a sinusoidal characteristic of OSPL with respect to HHC phasing. Some ϕ_{HHC}'s alleviate BVI and others deteriorate. This figure shows that ϕ_{HHC} =0deg is most effective on BVI noise reduction, which reduces the noise by about 3dB from that of no HHC case, and ϕ_{HHC} =30deg is the worst.

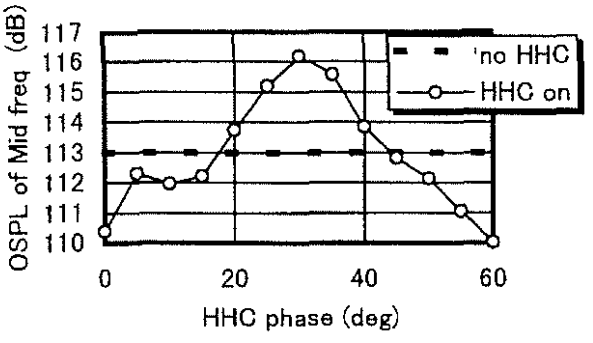

Fig.18 HHC effect on BVI noise in mid frequency OSPL of Mic#3

The sound pressure spectrum comparison among the best HHC case (ϕ_{HHC} =0deg), the worst HHC case (ϕ_{HHC} =30deg) and no HHC case are shown in Fig.19. It is noted that the two HHC-on cases, even the best HHC case, have larger SPL than no HHC case in less than 1000Hz. This is caused by larger loading noise generated by HHC operation. But this SPL magnitude order changes over 1000Hz range so that the magnitude order of SPL becomes consistent with the OSPL as shown in Fig.17 and Fig.18.

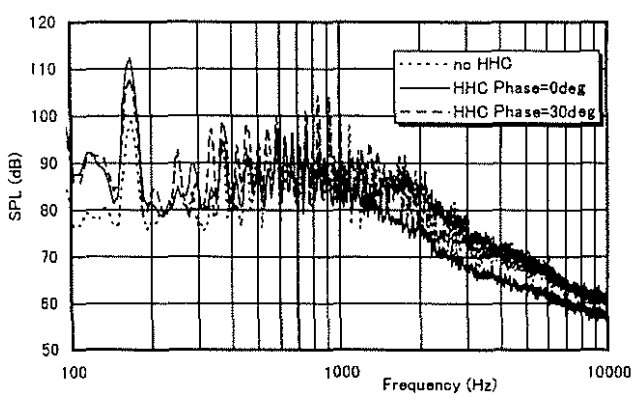

Fig.19 HHC effect on BVI noise spectrum of Mic#3

Fig.20 shows the unsteady blade surface pressure characteristics with respect to the rotor azimuth comparing with and without HHC cases. The pressure data presented here come from 4%c position of the upper surface at 6 blade span stations from 67%R to 95%R.

The no HHC case has the severe pressure fluctuation around ϕ =60deg and 300deg, which causes larger BVI noise as shown in Fig.17. But on the best HHC case for BVI noise reduction (ϕ_{HHC} =0deg), the pressure spikes on the advancing side are almost vanished. This change in the pressure characteristics between the two cases makes BVI noise reduction.

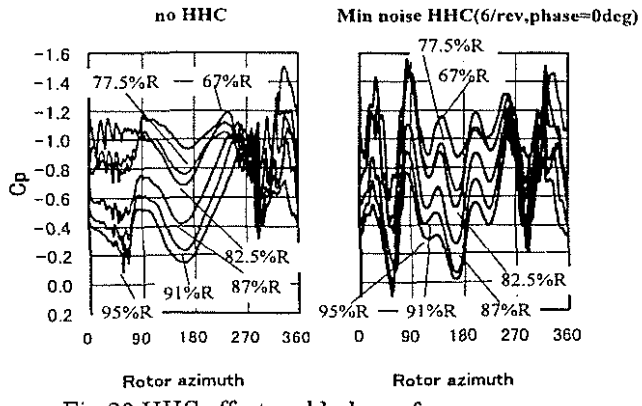

Fig.20 HHC effect on blade surface pressure at 4%c on upper surface

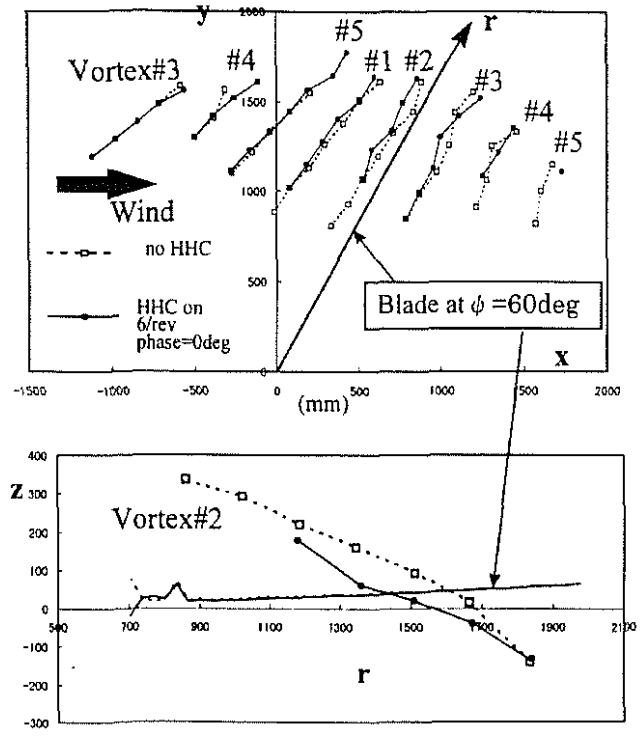

Fig.21 HHC effect on tip vortex trajectory with the blade at 60deg. azimuth position

The blade tip vortex trajectory obtained by LLS is shown in Fig.21 with the blade deformation measured by PGM comparing no HHC case and the minimum noise HHC case(ϕ_{HHC}=0deg).

Comparison between these two cases indicates that HHC application has a small influence on the horizontal trajectory of the tip vortex, but makes a large difference in the vertical trajectory projected on r-z plane at ϕ=60deg. Observing the trajectory of Vortex#2, which is just before the interaction with the reference blade at ϕ=60deg, it can be seen that no HHC case has the interaction at about 80%R and the minimum noise HHC case has at about 72%R.

It is inferred that this inward movement of the spanwise interacting position makes the difference in the degree of the smoothness of the Cp vs. ϕ curve shown in Fig.20 because of the difference of the spanwise blade local load between no HHC case and HHC on case at the interacting position. Then, the relief in SPL on the BVI region is made as shown in Fig.17. This inference will be verified later by evaluating the blade load distribution obtained by the pressure integration.

Fig.22 shows HHC influence on the rotor performance on BVI flight condition represented by C_Q and HHC phasing of 5/rev HHC as well as 6/revHHC. The increment in C_Q is more than 5% on 5/rev HHC with 0.7deg. amplitude and more than 1% on 6/rev HHC with 0.4deg. amplitude.
In both cases, the extra rotor power consumed by HHC is not fatal comparing to the rotor power of no HHC case. Furthermore, the flight condition which causes BVI is descending, where the required rotor power has a wide margin up to the engine available power. Consequently, it is predicted that HHC operation will not cause a significant rotor power penalty.

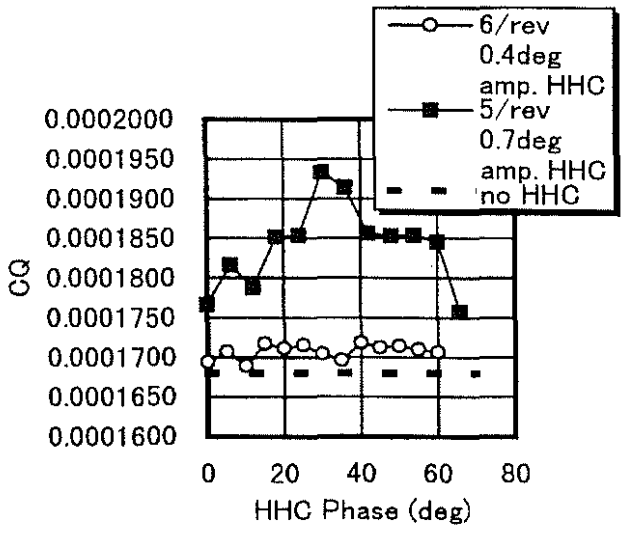

Fig.22 Influence of HHC on the rotor performance

Conclusion

(1)Sufficient data to evaluate ATIC's noise reduction techniques had been obtained in this wind tunnel testing.

(2)A part of data study for the effects of blade geometry, variable rotor rpm, rotor configuration and HHC on performance/noise is performed.

(3)Further effort for test data evaluation should be kept going.

Acknowledgments

The authors wish to express their thanks to Dr. Mercker and many DNW/NLR staff for their support to perform this wind tunnel test campaign and to the PIV team from DLR lead by Dr. Ehrenfried. Also our thanks to Mr. Archinal and Mr. Ingalsbe of DEI for their assistance to handle the model rotor system.

References

1. Kondo, N., Nishimura, H., Nakamura, H., Aoki, M., Tsujiuchi, T., Yamakawa, E., Aoyama, T., Saito, S., " Preliminary Study for a Low Noise Rotor ", 23rd European Rotorcraft Forum, Dresden , Germany, September 1997, Paper 22.

2. Nishimura, H., Kondo, N., Nakamura, H., Tsujiuchi, T., Yamakawa, E., Aoyama, T., Saito, S., " Comparison between Calculated Rotor Noise and Experimental Data obtained by DNW Test ", 24th European Rotorcraft Forum, Marseilles, France, September 1998, Paper AC06.

3. Hayama, K., Inagaki, K., Yamakawa, E., "Dynamic Stall Characteristics of a Helicopter Blade Tip ", Heli Japan 98, Gifu, Japan, April 1998, Paper No. T3-5.

4. Tsujiuchi, T., Nishimura, H., Kondo, N., Yamakawa, E., Aoyama, T., Saito, S., " Experimental and Numerical Study for Design of Blade vortex Interaction " Heli Japan 98, Gifu, Japan, April 1998, Paper No. T1-3.

5. Kobiki, N., Tsuchihashi, A., Murashige, A., Yamakawa, E., "Study for the effects of Active Flap on Blade Vortex Interaction ", Heli Japan 98, Gifu, Japan, April 1998, Paper No. T4-3.

6. Kobiki, N., Tsuchihashi, A., Murashige, A., Yamakawa, E., "Elementary Study for the Effects of HHC and Active Flap on Blade Vortex Interaction ", 23rd European Rotorcraft Forum, Dresden , Germany, September 1997, Paper 29.

7. Hongu, T., Sato, M., Yamakawa, E., "Fundamental Study of Smart Material Actuators for Active Flap Control ", Heli Japan 98, Gifu,

Japan, April 1998, Paper No. T6-1.

8. Nakamura, H., Nishimura, H., Kondo, N., Yamakawa, E., Aoyama, T., Saito, S., "Effect of Blade Geometry on BVI Noise in Various Flight Conditions ", Heli Japan 98, Gifu, Japan, April 1998, Paper No. T4-6.

9. Ochi, O., Shima, E., Yamakawa, E., Aoyama, T., Saito, S., " Aerodynamic and Aeroacoustic Analysis of BVI by Moving Overlapped Grid Method" , 24th European Rotorcraft Forum, Marseilles, France, September 1998, Paper AC04.

10. Tsuchihashi, A., Murashige, A., Tsujiuchi, T., Yamakawa, E., "Experimental Study of Blade-Tip Vortex ", Heli Japan 98, Gifu, Japan, April 1998, Paper No. T3-6.

11. Murashige, A., Tsuchihashi, A., Tsujiuchi, T., Yamakawa, E., " Blade-Tip Vortex Measurement by PIV ", 23rd European Rotorcraft Forum, Dresden , Germany, September 1997, Paper 36.

12. Yamakawa, E., Murashige A., Kobiki, N., Downs, G., Archinal, T., Ingalsbe, G., Gold, R., " Development of An Aero-Acoustic Model Rotor Test System for DNW Test ", Heli Japan 98, Gifu, Japan, April 1998, Paper No. T3-3.